Enhanced Stabilization and Deposition of Pt Nanocrystals on Carbon by Dumbbell-like Polyethyleniminated Poly(oxypropylene)diamine

ARTICLE *in* THE JOURNAL OF PHYSICAL CHEMISTRY B · JUNE 2006

Impact Factor: 3.3 · DOI: 10.1021/jp057560a · Source: PubMed

Enhanced Stabilization and Deposition of Pt Nanocrystals on Carbon by Dumbbell-like Polyethyleniminated Poly(oxypropylene)diamine

Wei-Fu Chen, Hsin-Yeh Huang, Chia-Hui Lien, and Ping-Lin Kuo*

Department of Chemical Engineering, National Cheng Kung University, Tainan, Taiwan 70101

Received: December 29, 2005; In Final Form: March 31, 2006

Pseudo-dendritic polyethyleniminated poly(oxypropylene)diamine (D400(EI)$_{20}$) was used as a stabilizer and promoter to prepare Pt nanoparticles in aqueous solution, which was then deposited on carbon surface followed by calcination. After being deposited on carbon surface, no Pt^0 could be detected in the solution phase. In all steps, the increasing molar ratio of the amino groups of D400(EI)$_{20}$ to H_2PtCl_6 ([N]/[Pt]) drastically reduced the size and the polydispersity and kept a constant low value after [N]/[Pt] = 20. Under a [N]/[Pt] ratio of 20, the particle sizes obtained from transmission electron microscopy (TEM) were very small in solution (2.7−2.4 nm) and remained the same after being deposited on carbon surface (2.7−2.4 nm), and were only slightly increased to 3.6−3.0 nm after calcination. The stabilizing ability of D400(EI)$_{20}$ to Pt on carbon surface before and after calcination can be interpreted by the existence of binding energy between Pt and amine nitrogen. The X-ray diffraction (XRD) pattern together with the TEM image reveals that the obtained Pt nanoparticles exist in single-crystal form. The results of photoelectron spectroscopy (XPS) evidence that the metallic Pt(0) rather than the oxidized Pt is the predominant species in the Pt/C catalysts. The electrochemical active surface (EAS) area of the Pt/C catalyst is only slightly higher than that of the E-TEK Pt/C catalyst, but the utilization factor (93.4%) is remarkably higher than the latter (62.8%). The increasing time of thermal treatment increases the crystallinity of Pt(0) on carbon, accompanied by the increasing EAS areas, which corresponds to its enhanced electrocatalytic performance to methanol oxidation.

Introduction

The preparation of nanoscopic platinum-based catalysts is now of interest because of their huge surface areas and unique properties that could make them useful in a wide range of applications.[1,2] One of the most interesting is the carbon-supported Pt-based catalyst, which is crucial for use in fuel cells.[3] It is known that the higher surface area, which relates to the increase of reacting sites, can be achieved when the dimension of particles decreases.[4] To effectively use these metals, they have to be well dispersed on conductive carbon supports in small size. Fuel cell catalysts are generally produced by the impregnation method in which a Pt precursor is impregnated into carbon black, followed by high-temperature oxidation and reduction. This method is simple and suitable for large-scale productions;[5] however, it is not adequate from the viewpoint of offering both high dispersion of metals on carbon and high quantity of effective Pt sites at the same time,[6] and furthermore the microporosity of the carbon support would limit the accessibility of deposited platinum to the fuel (e.g., hydrogen or methanol). Hence, the synthesis of such nanoparticles with good dispersion on the supporting materials remains to be challenging and tedious work. Many research groups have reported new fabrication strategies to achieve well-dispersed Pt particles over the supporting carbon. They have employed various kinds of stabilizing agents such as ammonium salts, PVP, and PVA, etc.,[7−11] or new organometallic precursors, for example, $Ru_5C(CO)_{14}Pt$-(COD) and $PtMe_2(\eta^4\text{-}C_8H_{12})$. The electrocatalytic performance of these catalysts was found to be equivalent or slightly higher than that of the commercial E-TEK catalyst.

In our laboratory, several kinds of pseudo-dendritic polyethyleniminated polymers were used as stabilizers to prepare metal nanoparticles.[12,13] The dumbbell-like ABA-type triblock polyethyleniminated poly(oxypropylene)diamine (D400(EI)$_{20}$) possesses poly(oxypropylene) as lipophile and pseudo-dendritic polyethylenimine as hydrophile. Therefore, it is expected that the hydrophile can effectively stabilize Pt(IV) and Pt(0) in solution and on carbon surface through the interaction between Pt(IV)/Pt(0) and unpaired electrons on nitrogen, and the lipophile can promote the D400(EI)$_{20}$ loaded with Pt(0) nanoparticles to adsorb onto carbon surface. Meanwhile, both lipophile as well as hydrophile can serve as blocks to successfully separate the generated nanoparticles to prevent the aggregation during the thermal activation process.

In this study, D400(EI)$_{20}$ was used as a stabilizer and promoter to prepare Pt nanoparticles in aqueous solution, which was then deposited on carbon surface followed by thermal activation. It was found that D400(EI)$_{20}$ very effectively stabilizes Pt(0) nanoparticles in each step and promotes the deposition of Pt(0) onto carbon. Under the protection of D400-(EI)$_{20}$, the obtained Pt(0) on carbon surface is small (3.6−3.0 nm), existing in single-crystal form, and exhibits a high utilization factor, where the photoelectron spectroscopy (XPS) evidences that the metallic Pt(0) rather than the oxidized Pt is the predominant species in the Pt/C catalyst. The bonding between D400(EI)$_{20}$ and surface Pt as well as the interaction between the amino groups on D400(EI)$_{20}$ and the carboxylic

* Corresponding author. Tel.: +886-6-275 7575 x62658. Fax: +886-6-276 2331. E-mail: plkuo@mail.ncku.edu.tw.

10.1021/jp057560a CCC: $33.50
Published on Web 05/02/2006

functionalities on carbon supports were investigated to look into the functions of D400(EI)$_{20}$.

Experimental Section

Materials. Polyethyleniminated poly(oxypropylene)diamine, D400(EI)$_{20}$, was prepared according to our previously reported procedures.[13] Hexachloroplatinic acid ($H_2PtCl_6 \cdot 6H_2O$) was purchased from Alfa Aesor. Nafion solution (5 wt %), carbon paper (Toray, 30 wt % wet-proofing), and commercial Pt catalysts (20 wt %) were provided by E-TEK, Inc. Vulcan XC-72 carbon used as the supports was obtained from Carbot (USA). Other chemicals including sodium hydroxide (NaOH), sodium borohydride ($NaBH_4$), methanol (CH_3OH), sulfuric acid (H_2SO_4), nitric acid (HNO_3), and isopropyl alcohol (IPA) were obtained from Aldrich. All aqueous solutions were prepared using deionized water purified through a Milli-Q system.

Synthesis of Carbon-Supported Pt(0)−D400(EI)$_{20}$ Colloids. The normality molar ratio of the amine groups on D400(EI)$_{20}$ to metal precursor was denoted as [N]/[M]. Four catalysts with [N]/[Pt] molar ratios of 5, 10, 20, and 50 were synthesized by mixing corresponding 0.5, 1.0, 2.0, and 5.0 mmol of D400(EI)$_{20}$ with 0.1 mmol of H_2PtCl_6 in 100 mL of deionized water to form yellow suspensions. The pH value was adjusted to around 9.2 by addition of 0.1 N NaOH aqueous solution. Next, 5×10^{-4} mol of $NaBH_4$ was added dropwise to each suspension with vigorous stirring. The color of the resulting solutions changed to brown within 30 min, indicating the formation of Pt nanoparticles.

The Pt/C catalysts were prepared by combining Pt colloidal solutions with a suspension of Vulcan XC-72 ($S_{BET} = 236.8$ $m^2\ g^{-1}$) in water. The Vulcan XC-72 carbon was pretreated with 67% HNO_3 at 80 °C for 24 h, was dispersed in deionized water and filtered, and was then washed with deionized water several times. The dispersion, filtering, and washing steps were repeated until the pH of the filtrate reached 7. The filtered cake was eventually dried under vacuum at 80 °C for 24 h, giving carboxyl-functionalized carbon black. A nominal metal loading of 20 wt % was taken on all of the catalysts. The solutions were stirred vigorously for 1 h, and then centrifugation process was performed to separate the solid residue and solvent at a speed of 5000 rpm for 30 min. The resulting solids were washed with a copious amount of distilled water to remove excess Cl^- and finally dried in an oven at 90 °C. The filtrate was colorless and analyzed with an inductively coupled plasma atomic emission spectrometer (ICP-AES), indicating that almost all Pt was adsorbed on the carbon black.

Thermal Activation and Preparation of Pt/C Nanocatalyst. The thermal decomposition temperature, defined as the temperature at 10 wt % weight loss ($T_d^{0.1}$), was determined by the TGA thermogram of D400(EI)$_{20}$ (see Figure S1a) to be about 325 °C. We chose 360 °C as the temperature of the thermal activation process to decompose D400(EI)$_{20}$ more effectively. The thermogram at the end was kept stable for at least 45 min and reached steady state (Figure S1b). The catalysts were calcined for 1, 3, 5, 10, and 15 h and then ground slightly in agate mortar. The resulting powder was used to prepare working electrodes.

The working electrode is a thin layer of Nafion-impregnated catalyst cast on a vitreous carbon disk with 1 cm^2 of the surface area. The Pt loading of the working electrode was fixed at 1 mg cm^{-2}. The catalyst powder was dispersed in 2-propanol and stirred vigorously for 1 h. Next, 2.5 wt % Nafion solution was added into the slurry by keeping the ratio of catalyst to Nafion (dry) at 1:3. After ultrasonication for 1 h, the resulting ink was spread on carbon disk and dried under vacuum at 60 °C for 3 h.

Characterizations. The morphology, size, and size distribution of these catalysts were characterized by transmission electron microscopy (TEM) using a JEOL JEM-1200CX-II microscope operating at 120 kV. Specimens were prepared by placing a drop of the colloidal dispersion onto 200-mesh copper grids coated with an amorphous Formvar carbon film, and dried overnight at room temperature in a vacuum oven before introducing the grid into the microscope. TG analysis was performed on a thermogravimetric analyzer (Perkin-Elmer TGA 7) in N_2 for carbon-supported catalysts.

X-ray photoelectron spectroscopy (XPS) measurements were carried out with a VG Scientific ESCALAB 210 electron spectrometer using Mg Kα radiation under a vacuum of 2×10^{-8} Pa. Narrow scan photoelectron spectra were recorded for the C 1s, O 1s, N 1s, and Pt 4f regions and analyzed by deconvolution to estimate the surface oxidation states of the catalysts. X-ray powder diffraction (XRD) was performed on a Rigaku RINT2100 X-ray diffractometer with Cu Kα radiation ($\lambda = 0.1524$ nm) operated at 40 kV and 40 mA by placing the powder of carbon-supported catalysts onto a glass slide.

A CHI-608A potentiostat/galvanostat and a conventional three-electrode test cell were used for electrochemical measurements. Pt wire and Ag/AgCl electrode were used as the counter and reference electrodes, respectively. All electrolyte solutions were degassed by purging N_2 for 3 h prior to every measurement. The cyclic voltammetry (CV) experiments were performed in a 0.5 M H_2SO_4 solution in the absence and presence of 1 M CH_3OH at 20 mV/s. Stable voltammograms recorded after at least 20 cycles were taken into account for data interpretation.

Results and Discussion

Stabilizing Effect of D400(EI)$_{20}$ on Pt Nanocrystals in Solution and on Carbon Surface. ABA-type triblock copolymers, polyethyleniminated poly(oxypropylene)diamine (D400(EI)$_n$), were used to prepare noble metal nanoparticles in our previous work.[11] In this study, they are employed as stabilizers and promoters through the ethylenimine groups ($n = 20$) of two terminals of the poly(oxypropylene)diamines to prepare carbon-supported Pt nanocatalysts. Stabilization of the Pt particles by D400(EI)$_{20}$ can be discussed mainly from the viewpoint of complexing ability and steric effect. On one hand, amino-containing dendrimers or pseudo-dendritic polymers, which have been reported to interact with metal ions as well as with the corresponding reduced metal,[12−15] can be considered as a highly effective chelating agent to metal atoms, and, on the other hand, the poly(oxypropylene) chain surrounding the complexed metal core prevents the particles from undergoing any kind of agglomeration.

To evaluate the morphological effect of the D400(EI)$_{20}$ concentration, a series of Pt colloids was prepared by altering molar ratios of [N]/[Pt] from 5 to 50. Figure 1a is the typical image of the Pt colloid with a [N]/[Pt] ratio of 5, showing considerable aggregates composed of Pt nanocrystals with mean size of 3.6 ± 0.9 nm. The increasing of D400(EI)$_{20}$ concentration, for example, [N]/[Pt] = 20, induces drastic changes in both the morphology and the size of these nanocrystals (Figure 1d). No longer seen are the agglomerated particles; instead, remarkably uniform nanocrystals with smaller sizes (2.7 ± 0.6 nm) are found to be distributed in a highly dispersed fashion. The decreased agglomeration can be explained by that an excess of D400(EI)$_{20}$ more effectively covers or encapsulates more Pt

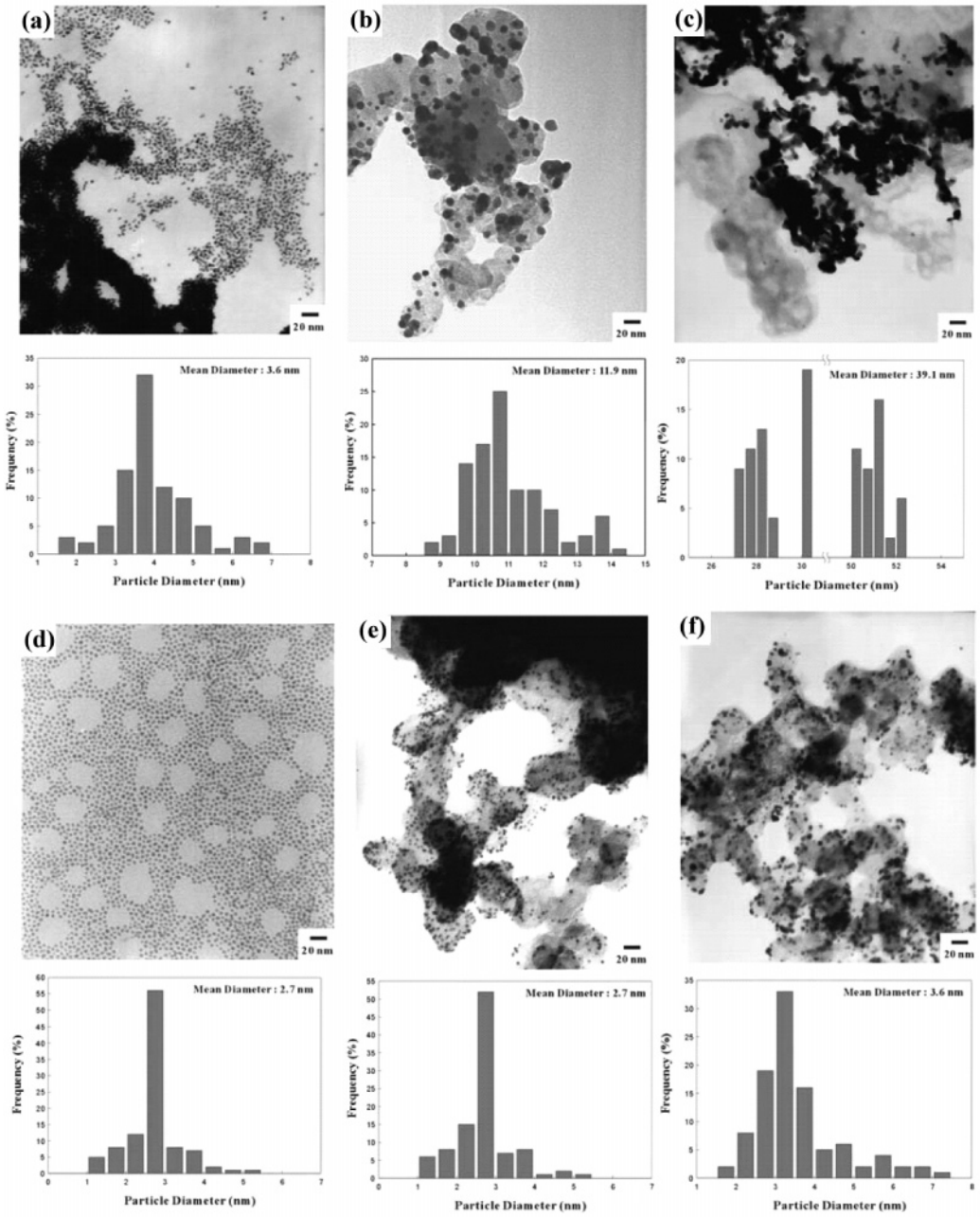

Figure 1. TEM images of the Pt nanocrystals with (a) [N]/[Pt] ratio = 5 and (d) [N]/[Pt] = 20. The Pt nanoparticles after depositing on carboxyl-functionalized Vulcan XC-72 carbon with (b) [N]/[Pt] = 5 and (e) [N]/[Pt] = 20. The thermal activated Pt/C catalysts with (c) [N]/[Pt] = 5 and (f) [N]/[Pt] = 20.

nanocrystals and decreases the attractive interactions between nanocrystals to keep them apart, resulting in the formation of well-distributed Pt colloids.

Oxygen-containing carbon black can be prepared by oxidizing Vulcan-XC72 carbon black with a high concentration of HNO_3[16,17] to produce a great amount of carboxyl groups on the carbon surface, which results in an interaction between the carboxyl groups and the Pt(0)−D400(EI)$_{20}$ macromolecules. The "free" amine groups on Pt(0)−D400(EI)$_{20}$ can further attach onto the carbon surface through electrostatic interaction and/or hydrogen-bonding force with the surface carboxyl groups, as shown in Scheme 1. The hydrophobic poly(oxypropylene) segments can also promote D400(EI)$_{20}$ loaded with Pt nanoparticles to adsorb onto carbon surface through hydrophobic interaction and meanwhile separate the particles from each other. Moreover, during the thermal activation process, these macromolecules can also serve as blocks to effectively prevent metal particles from aggregation or fusion. When we examine the deposition process of Pt(0)−D400(EI)$_{20}$ from the colloidal solution with a [N]/[Pt] ratio of 20 onto the carbon surface, the presence of D400(EI)$_{20}$ is confirmed by the C 1s, O 1s, and the more evident N 1s lines in the XPS spectra. The surface of carbon black has been partially carboxyl-functionalized after the HNO_3 treatment, as indicated by the presence of the carbonyl carbon at 288.0 eV, which is attributed to COOH and COOR groups, and C−H component at 284.9 eV in the C 1s spectrum in Figure 2a.[18] Another component at 285.9 eV is attributed to the C−N functionality in D400(EI)$_{20}$.[19] The O 1s line in Figure 2b is found to consist of three nearly superimposed signals. The first at 531.9 eV indicates the existence of Pt−O species.[20] The other two peaks are assigned to carbonaceous species, including ether-like species (C−O) at 533.2 eV corresponding to the ether oxygen of poly(oxypropylene) chain and the carboxyl oxygen (C═O) at 534.1 eV.[21] When Pt(0)−D400(EI)$_{20}$ macromolecules

SCHEME 1

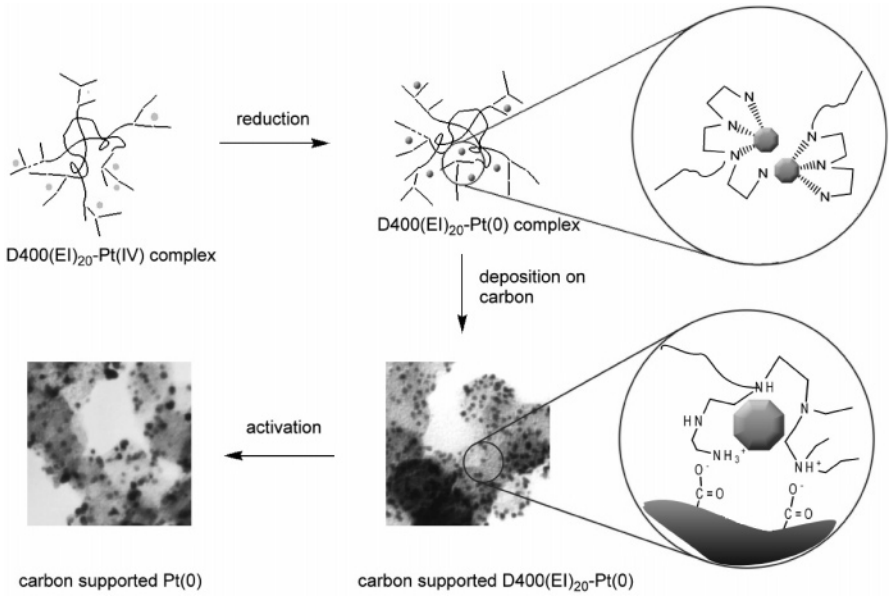

attach to the carbon surface, the free amino moieties are available for charge transfer with substrate carboxyl groups to form the $-COO^{-}NH_3^{+-}$ functionality. These primary ammonium ions correspond to the peak component at 401.1 eV in the N 1s spectrum as shown in Figure 2c.[22] A prominent N 1s signal also appears at 399.1 eV, which is attributed to the free amine groups.[23] Adsorption of the stabilizing layer over the surface of the Pt particles through the head-on N atom is evidently observed by the peak component at 397.5 eV, which is assigned to a nitride bonding (Pt−N).[24,25] These results have provided sufficient evidence for the presence of N atoms that could have coordination affinity with the Pt atoms and electrostatic interaction with carboxyl groups on the surface of carbon black.

Adsorption of the colloidal Pt particles on HNO_3-treated Vulcan XC-72 carbon brings about significant morphological changes for the sample with a [N]/[Pt] ratio of 5 (Figure 1b). A large number of agglomerated particles with average diameter of 11.9 ± 1.2 nm are obtained. In contrast, the Pt nanocrystals on carbon surface with a [N]/[Pt] ratio of 20 have a smaller mean particle size (Figure 1e) and show a homogeneous dispersion with a narrower size distribution (2.7 ± 0.6 nm). The mean diameters and corresponding standard deviations of the D400(EI)$_{20}$-stabilized Pt nanocrystals supported or unsupported on Vulcan XC-72 carbon with [N]/[Pt] ratios from 5 to 50 are shown in Table 1. It is clear that the average size of the Pt nanocrystals decreases with increasing [N]/[Pt] ratios, reaching a plateau at a [N]/[Pt] ratio of 10 for both the unsupported and the carbon-supported cases. The addition of a significant excess of amine seems to greatly assist in the formation of smaller and uniform nanocrystals. A rational explanation for this optimum in size found with a [N]/[Pt] ratio of 10 is that there is an optimal size for the nanocrystals that allows a most stable packing[26] arrangement for the capped D400(EI)$_{20}$ chains. It is noteworthy in the case of [N]/[Pt] = 5 that after being supported on carbon, the particle size increases from 3.6 to 11.9 nm. The explanations of this increase in particle size are stated as follows.

Before deposition onto carbon, the interaction between the platinum and the amino group has been clearly evidenced by the existence of Pt−N bonding as shown in Figure 2c. This interaction results in the decrease in the surface energy of Pt particles. After the carboxyl-functionalized carbon was added, the occurred interaction between the amino groups on polymer and the carboxylic groups on carbon surface decreased the effective amount of amino groups attached on the Pt surface, resulting in an increase of the surface energy of Pt, in turn, to cause the aggregation of Pt nanoparticles. However, as the ratio of D400(EI)$_{20}$ was increased ([N]/[Pt] ratio is higher than 5), the particle size did not apparently increase in the presence of carbon. Sufficient polyethylenimine chains can well protect Pt particles through the interaction between amino groups and platinum as demonstrated by XPS. This demonstrates that the existence of polymer protects Pt nanoparticles from aggregation.

Stabilizing Effect of D400(EI)$_{20}$ during the Thermal Activation Process. XPS measurements have been undertaken to probe for the presence of organic components on metal particles.[27] In the present study, the removal of the stabilizing shell during the thermal activation process was examined by the N 1s line for the D400(EI)$_{20}$-stabilized Pt/C colloids. Figure 3a shows the spectral region of the N 1s band for the carbon-supported Pt(0)−D400(EI)$_{20}$ colloids ([N]/[Pt] = 20) before (curve i) and after thermal treatment at 360 °C for 10 h (curve ii) and 15 h (curve iii). The N 1s signal decreases considerably to the level of a trace signal after 10 h, suggesting accomplishment of the removal of the nitrogenous species.

Although the thermal activation of the catalysts allows the Pt nanocrystals to expose their active sites, it is the state of the surface Pt atoms that determines the activity of Pt-based catalysts. In Figure 3b, the Pt 4f line shows two pairs of doublets from the spin−orbital splitting of the $4f_{7/2}$ and $4f_{5/2}$. The most intense doublets observed, those at 71.2 and 74.5 eV, are attributed to zerovalent platinum (Pt(0)). The second set of doublets obtained at 72.6 and 76.7 eV can be ascribed to Pt(II) chemical states such as the PtO and $Pt(OH)_2$ species,[28] indicating the presence of Pt oxides. The percentage of each component is obtained from the relative area of these peaks. As shown in Table 2, the percentages of Pt(0) are given as 73.83% for the Pt/C catalyst; this figure is equal to that of the E-TEK Pt/C catalyst, 73.54%,[6a] which can be used to prepare metallic Pt-(0)-dominated catalysts.

The morphology of the Pt/C catalysts heat-treated for 10 h having the [N]/[Pt] ratios of 5 and 20 was shown in Figure 1c and f. At the lower [N]/[Pt] ratio of 5, extremely severe

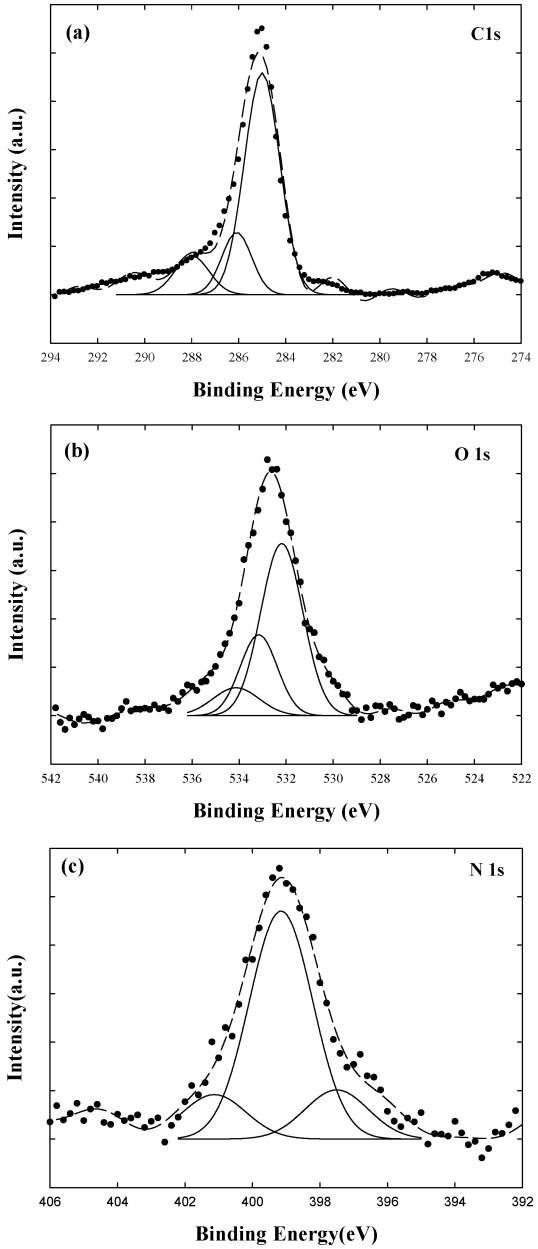

Figure 2. X-ray photoelectron spectra of the Pt/C colloids before thermal treatment in the (a) C 1s, (b) O 1s, and (c) N 1s regions (●, raw data; - - -, fit data; −, deconvoluted data).

TABLE 1: Mean Diameters and Standard Deviations of Pt Nanoparticles, and As-Prepared and Heat-Treated Pt/C Catalysts with Different [N]/[Pt] Ratios

[N]/[Pt]	Pt particles, d_p (nm)	Pt particles on carbon, d_c (nm)	heat-treated Pt/C, d_h (nm)[a]
5	3.6 ± 0.9	11.9 ± 1.2	39.0 ± 8.4
10	2.9 ± 0.7	2.9 ± 0.7	5.7 ± 1.6
20	2.7 ± 0.6	2.7 ± 0.6	3.6 ± 1.1
30	2.5 ± 0.6	2.5 ± 0.6	3.2 ± 0.9
40	2.5 ± 0.7	2.5 ± 0.7	3.3 ± 0.9
50	2.4 ± 0.5	2.4 ± 0.5	3.0 ± 0.8

[a] The Pt/C catalyst after thermal activation at 360 °C under N_2 for 10 h.

coalescence of the particles takes place, leading to a significant enlargement of particle size from 11.9 to 39.0 nm. In contrast, the Pt/C catalyst formed with a [N]/[Pt] ratio of 20 followed by the thermal activation does not show significant morphologic changes (from 2.7 to 3.6 nm). The average sizes and corresponding standard deviations of the heat-treated Pt nanocrystals

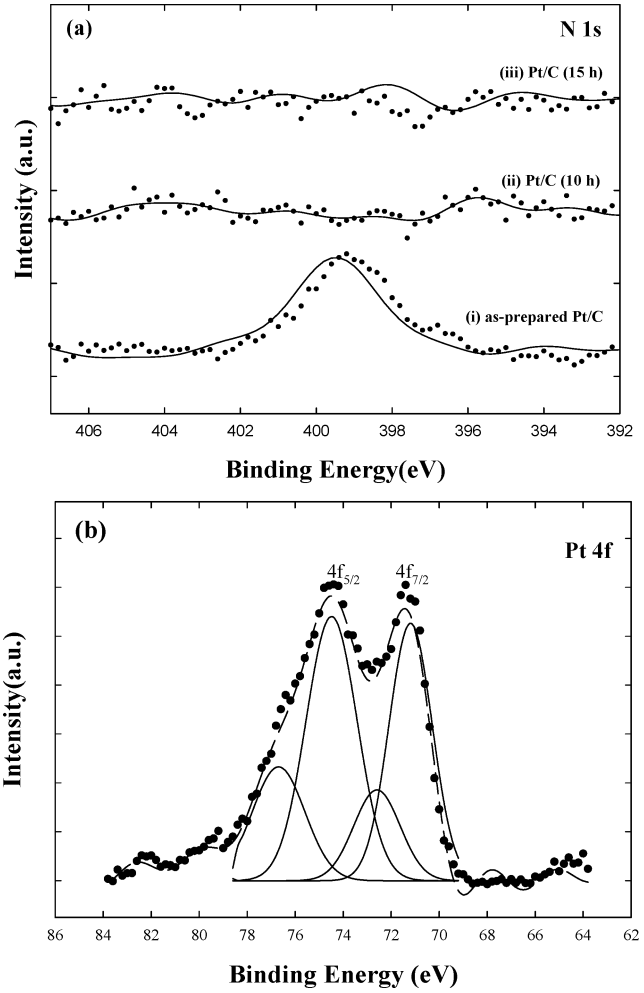

Figure 3. XPS spectra of (a) N 1s lines for Pt/C catalysts ([N]/[Pt] = 20) with different thermal activation times and (b) Pt 4f region for Pt/C catalyst ([N]/[Pt] = 20) after thermal activation for 10 h (●, raw data; - - -, fit data; −, deconvoluted data).

TABLE 2: Binding Energy and Relative Intensity of Different Species from Curve Fitted X-ray Photoelectron Spectra in the Pt/C Catalysts

spectra	binding energies (eV)		species	relative intensity (%)
C 1s	285.0		−C−H	71.1
	286.1		−C−N−	16.8
	288.0		−COO−	12.1
O 1s	531.9		Pt−O−	61.2
	533.2		−C−O−	28.8
	534.1		−C=O	10.0
N 1s	397.5		Pt−N−	
	399.1		free amine	
	401.1		$-NR_4^+$	
Pt 4f	71.19	74.48	Pt(0)	73.8
	72.59	76.69	Pt(II)	26.2

supported on carbon with [N]/[Pt] ratios from 5 to 50 are also shown in Table 1. Both average diameters and standard deviations increase as compared to those before the thermal activation process. The dependence of the average sizes of Pt/C colloids before and after thermal activation on [N]/[Pt] ratios is plotted in Figure 4. The decreasing trend of particle size as a function of [N]/[Pt] ratio can be obtained from the monotonically decreasing curve toward higher [N]/[Pt] ratios. Obviously, the decreasing degree for heat-treated Pt/C is much higher than that for untreated ones until the [N]/[Pt] ratio of 20. Because the XPS and TGA results indicate the complete removal of the

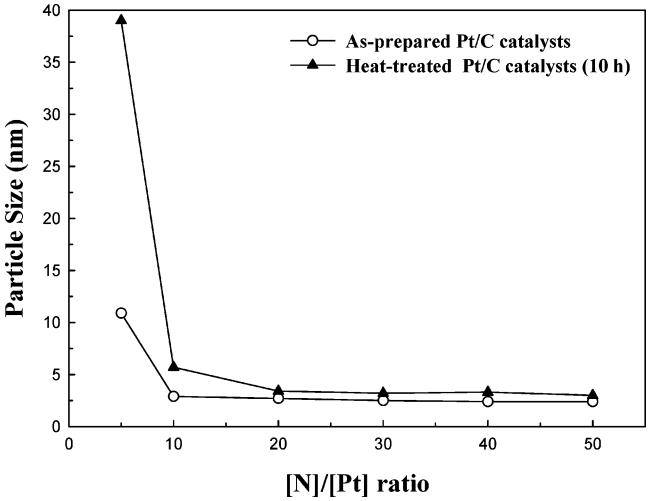

Figure 4. The dependence of particle sizes on the [N]/[Pt] ratios for the as-prepared and thermal activated Pt/C catalysts.

$D400(EI)_{20}$ molecules at [N]/[Pt] = 20, some kind of stabilizing mechanism provided by $D400(EI)_{20}$ should exist during the thermal activation process to prevent particles from aggregation and limit their growth. We propose that the gradual decomposition of $D400(EI)_{20}$ existing on the Pt surface results in the formation of chars, which serves as a block to effectively prevent further coalescence of these particles. This explanation will be verified by the stabilization effect with altered thermal activation time in the following section. Furthermore, the average size has reached a plateau at [N]/[Pt] = 20, indicating an optimal condition for preparing Pt/C nanocatalyst in the present process.

Effect of Thermal Activation Time. The influence of thermal activation time on the carbon-supported Pt nanocrystals ([N]/[Pt] = 20) was evaluated by TEM analysis and XRD patterns. Figure 5a−e displays the TEM images of these Pt/C colloids after thermal activation at 360 °C for 1, 3, 5, 10, and 15 h under N_2. The comparable E-TEK 20 wt % Pt/C sample is also shown in Figure 5f. It is found that no remarkable morphological change occurs with increase of the activation time. Even for the case of 15 h, only a few coagulations of particles are observed, and its average size (4.6 nm) is only slightly larger than those of the 10 h (3.7 nm) and the E-TEK catalyst (3.2 nm). This indicates that after the $D400(EI)_{20}$ is entirely decomposed, the Pt particles are still stabilized. It is well documented now that the stabilization on Pt particles during thermal activation is highly dependent on the quantity of stabilizers $D400(EI)_{20}$, and the residual chars on the Pt surface formed during thermal activation result in an increase in the activation energy required for particle aggregation through surface diffusion. The powder XRD patterns of the same Pt/C catalysts are presented in Figure 6a. Despite the graphite peaks at 20−25°, the characteristic diffraction peaks at 39°, 46°, 67°, 81°, and 86° are designated to the Pt {111}, {200}, {220}, {311}, and {222} facets of the face-centered cubic (fcc) crystal structure, respectively.[29] The lattice constants in all cases (i.e., 3.921 Å) are in good agreement with that of 3.923 Å for pure Pt. The Pt {111} peaks become sharper and more intense as activation time increased, suggesting a significant enhancement on the degree of crystallization due to the thermal effect. The grain sizes (d_{XRD}) were obtained by measuring the broadening of the {111} peaks and applying the Scherrer equation,[30]

$$d\ (\mathrm{nm}) = \frac{k\lambda}{\beta \cos \theta}$$

where k is a constant (0.0368 nm), λ denotes the wavelength of X-ray used (0.154 nm), β is the full-width half-maximum (fwhm) of the respective diffraction peak (rad), and θ is the angle at the position of peak maximum (rad). The calculated sizes of the particles with activation times of 0, 1, 3, 5, 10, and 15 h are 2.0, 2.2, 2.5, 2.6, 3.3, and 3.6 nm, respectively. The dependence of the average particle size, determined from TEM and XRD measurements, on the thermal activation time is shown in Figure 6b. The relationship between particle size and thermal activation time obtained from TEM is similar to that from XRD, indicating that the obtained Pt particles are mainly composed of single crystals. In summary, the thermal activation process not only removes $D400(EI)_{20}$ but also improves the crystallinity of the Pt/C catalysts. It has been known that specific crystal planes of Pt nanocrystals (Pt{110} and Pt{100}) can facilitate adsorption of hydrogen and methanol and favor dissociation of adsorbed methanol during the oxidation reaction.[31]

Electrocatalytic Activity of Pt/C Catalysts. Cyclic voltammetry (CV) was employed to evaluate the electrochemical active surface (EAS) areas of the Pt/C catalysts with different thermal activation times in an electrolyte containing 0.5 M H_2SO_4, as displayed in Figure 7a. The as-prepared catalyst displays a featureless voltammogram with very small current density in the hydrogen adsorption−desorption region (−0.1 to 0.4 V), indicating that the covered $D400(EI)_{20}$ stabilizing shells completely block the active sites on the Pt nanoparticles. When the thermal activation at 360 °C is applied on the Pt/C catalysts for 10 h, a well-defined feature is observed due to the complete decomposition of $D400(EI)_{20}$ from the Pt surface, which agrees with the results of XPS and TG analysis discussed above.

The EAS areas (A_e) are calculated by measuring the amount of charge (Q_H) exchanged from the hydrogen desorption peaks after subtracting the contribution from the double layer region (assuming that the smooth Pt electrode gives a hydrogen adsorption charge of 210 μC cm^{-2}).[32] As listed in Table 3, A_e increases from 11.2 to 56.8 m^2/g Pt with increasing activation time from 1 to 15 h. The nominal surface area (A_n) is calculated by the equation: $6/d\rho$, where d is the average diameter of Pt nanocrystals, and ρ denotes the density of bulk Pt. From the ratio of measured EAS area and nominal surface area, A_e/A_n, the utilization factor (η), also shown in Table 3, can be calculated. The utilization factor increases linearly with the increasing activation time, strongly confirming the successful removal of the coverage of $D400(EI)_{20}$ on active Pt sites during the activation process. It is found that 93.4% of the surface Pt sites for the catalyst of 15 h are active for electrocatalysis; even the one of 10 h catalyst (68.5%) is higher than that of the E-TEK (62.8%). By the disappearance of the N 1s peak in the previous XPS analysis, we have known that the poisoning nitrogenous species over Pt surface has been completely removed at 10 h. The EAS area only increased a little from 51.8 m^2/g of 10 h to 56.8 m^2/g of 15 h, while the utilization factor changed greatly from 68.5% to 93.4%. Because the utilization factor is the ratio of active area over nominal surface area, this indicates a decrease in nominal surface area, that is, fewer sites resulting from the increase in particle diameter.

Figure 7b shows representative cyclic voltammograms (−0.2 to 1.0 V, 20 mV s^{-1}) of these Pt/C catalysts for methanol electrooxidation in 0.5 M H_2SO_4/1 M CH_3OH. For the as-prepared catalyst (the inset in Figure 7b), a very poorly resolved feature due to the coverage of $D400(EI)_{20}$ on Pt sites appears. After thermal activation, the oxidation current increases for all of the Pt/C catalysts until the potential reaches 0.69 V and starts to decrease because the formation of Pt oxides inhibits methanol

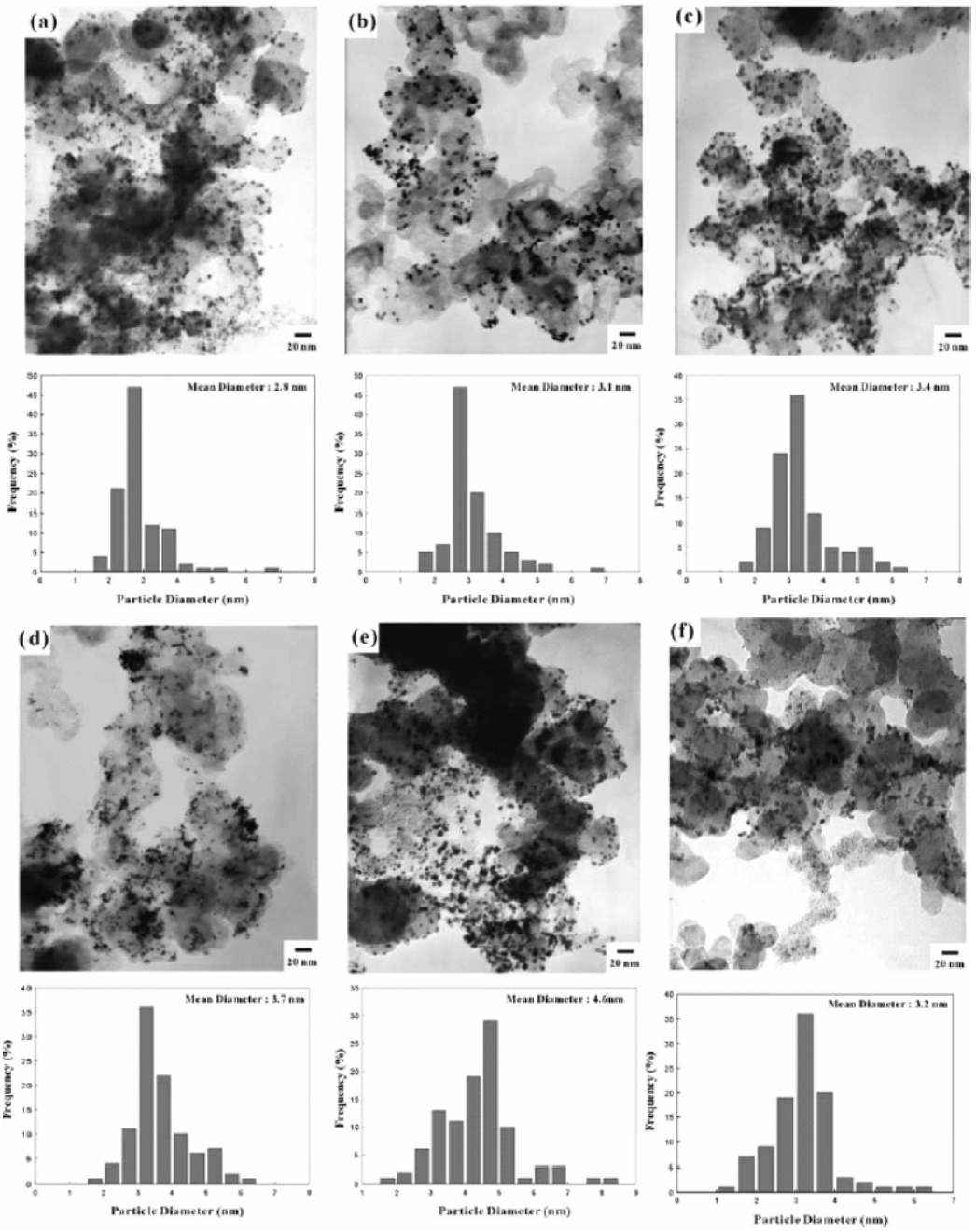

Figure 5. TEM micrographs and corresponding size histograms of the Pt/C catalysts ([N]/[Pt] = 20) with different thermal activation times: (a) 1 h, (b) 3 h, (c) 5 h, (d) 10 h, and (e) 15 h. The image of E-TEK Pt/C catalyst is also shown in (f).

TABLE 3: CV Results of the Pt/C Catalysts with Different Thermal Activation Times (1, 3, 5, 10, and 15 h)

treated time (h)	Q_H (mC/mg Pt)[a]	A_e (m^2/g)[b]	A_n (m^2/g)[c]	η (%)[d]	onset potential (V)	E_p (V)	I_f (A/mg Pt)
1	23.5	11.2	99.9	11.2	0.49	0.70	0.051
3	43.4	20.7	90.2	22.9	0.39	0.70	0.115
5	71.9	34.2	82.3	41.6	0.32	0.69	0.164
10	108.7	51.8	75.6	68.5	0.27	0.69	0.215
15	119.2	56.8	60.8	93.4	0.26	0.69	0.266
E-TEK	115.3	54.9	87.4	62.8			

[a] The amount of charge exchanged during the desorption of hydrogen on Pt sites. [b] Real surface area obtained electrochemically per gram of catalyst. [c] Nominal surface area calculated by the mean diameter. [d] Utilization factor = A_e/A_n.

oxidation at this higher potential range.[33,34] The peak current density (I_f) increases from 0.051 to 0.266 A/mg Pt with the increasing thermal activation time from 1 to 15 h as shown in Table 3, indicating that the improvement of catalytic activity follows the extent of decomposition of D400$(EI)_{20}$. On the negative sweep, anodic peaks at 0.44 V are observed. This anodic peak is generally accepted to be a consequence of the reoxidation of methanol after the reduction of the surface Pt oxides occurs.[35,36] A trend of negative shift for onset potential with increasing thermal activation time can also be seen in Table

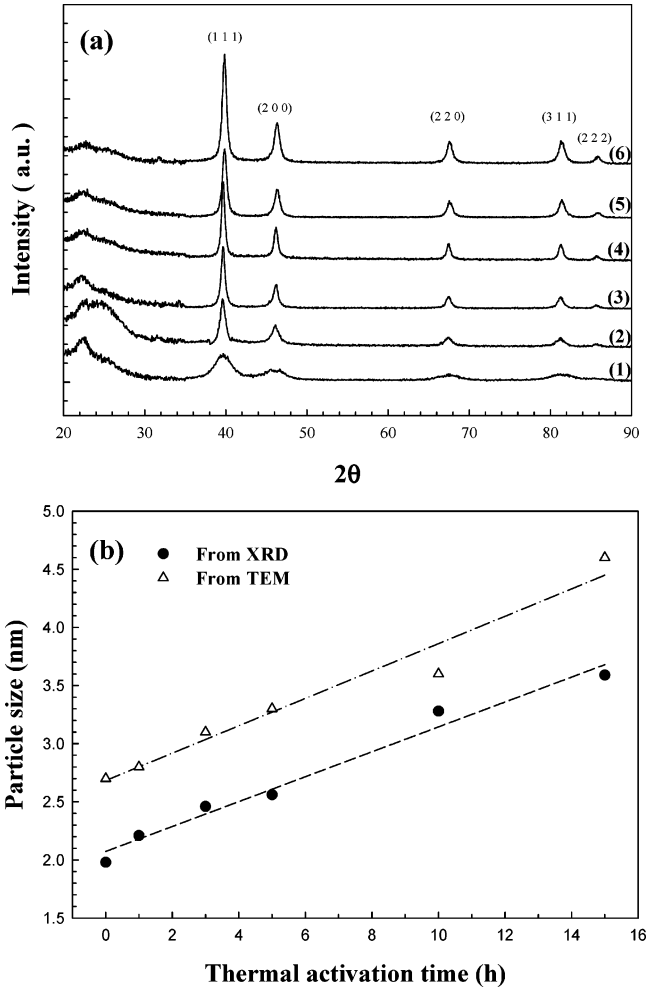

Figure 6. (a) X-ray diffraction patterns of the Pt/C catalysts ([N]/[Pt] = 20) with different thermal activation times: (1) as-prepared, (2) 1 h, (3) 3 h, (4) 5 h, (5) 10 h, and (6) 15 h. (b) The dependence of the thermal activation time on the particle sizes obtained from XRD and TEM.

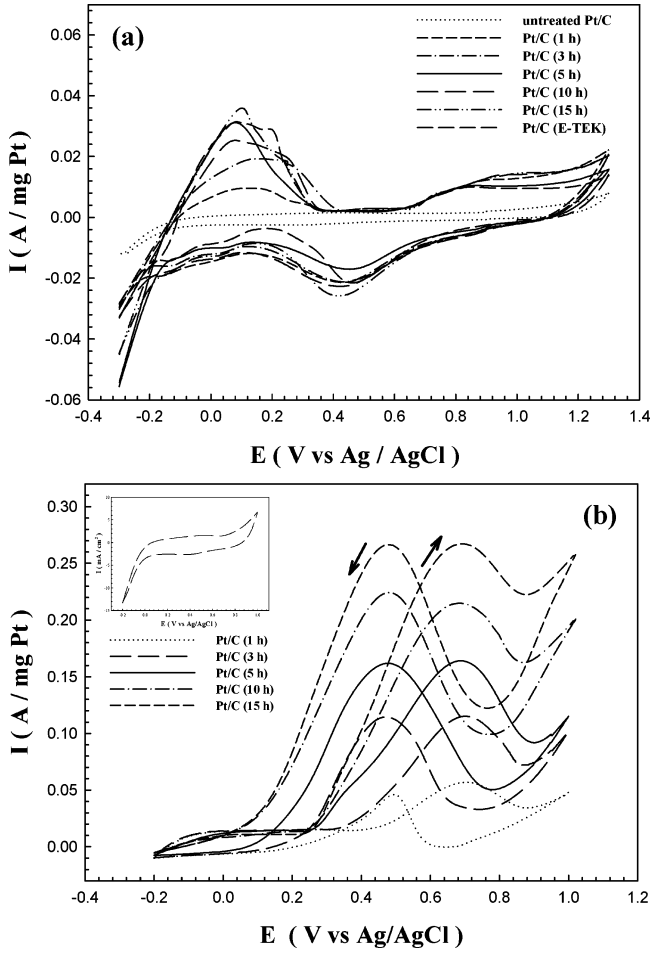

Figure 7. (a) Cyclic voltammograms of the Pt/C catalysts ([N]/[Pt] = 20) with different thermal activation times of 1, 3, 5, 10, and 15 h as well as the E-TEK catalyst in 0.5 M H_2SO_4 at 10 mV s^{-1}. (b) Cyclic voltammograms of the Pt/C catalysts ([N]/[Pt] = 20) with thermal activation times of 1, 3, 5, 10, and 15 h in 0.5 M H_2SO_4/1 M CH_3OH at 20 mV s^{-1}. The inset displays a cyclic voltammogram of the untreated Pt/C colloids.

3. This phenomenon is interpreted by that much lower activation energy is required to initialize the electro-oxidation of methanol after more complete removal of the stabilizing layers. For the catalyst of 15 h, a relatively negative onset potential (0.26 V) and a peak current density for methanol oxidation (0.266 A/mg Pt) similar or higher than those values reported in the literature are obtained. For example, the Vulcan XC-72 supported Pt catalysts synthesized by using TOAB as the stabilizer[9,10] have a very low onset potential of 0.22 V vs Ag/AgCl and a peak current density of 0.23 A/mg Pt in 0.5 M H_2SO_4/1 M CH_3OH solution. Liu et al. have reported that the Pt/C catalyst prepared by a microwave-assisted polyol process possesses 0.31 V vs SCE of onset potential and 0.27 A/mg Pt of peak current density in 1 M H_2SO_4/2 M CH_3OH electrolyte.[37] These results indicate that the D400$(EI)_{20}$ molecule attached on the Pt surface by its dendritic amino groups provides an excellent stabilizing effect, enhances the deposition of Pt nanocrystals onto carboxyl-functionalized carbon, and then separates the Pt particles from each other during the thermal activation process by increasing the activation energy for diffusion. The Pt/C catalysts with activation time higher than 10 h, which possess predominantly Pt(0) species on the crystal's surface, nanoscopic particle size, high crystallinity and EAS area, superior utilization factor, and high electrocatalytic performance in methanol oxidation should be a promising candidate for application in fuel cells.

Conclusion

The synthesis of Pt nanocrystals supported on the carboxyl-functionalized Vulcan XC-72 carbon has been achieved with the aid of the D400$(EI)_{20}$ molecules by the electrostatic force between the amino groups on D400$(EI)_{20}$ and the carboxyl functionalities over carbon surface and the hydrophobic interaction between the lipophile of D400$(EI)_{20}$ and the carbon surface. The average size of the carbon-supported Pt nanocrystals decreases with increase of the [N]/[Pt] ratios, reaching a plateau at a [N]/[Pt] ratio of 10. After the thermal activation process, extremely serious aggregation of the particles occurs at a [N]/[Pt] ratio of 5, leading to the enlargement of the mean diameter from 10.9 to 39.0 nm. For the [N]/[Pt] ratio higher than 20, the growth of the particle size is restricted even with an activation time of 15 h (from 2.7 to 4.6 nm), indicating an optimum value of the [N]/[Pt] ratio for the heat-treatment. A significant amount of Pt(0) species is obtained in the Pt 4f XPS spectrum for the catalyst with a [N]/[Pt] ratio of 20 heat-treated at 360 °C for 10 h (73.8%), these values being equal to that of the commercial E-TEK Pt/C catalyst (73.5%). The XPS spectrum in the N 1s region has proved the interaction between D400$(EI)_{20}$ and Pt particles by the Pt−N bonding and the subsequent removal from the Pt surface during the thermal activation process by the absence of the N 1s line.

The electrocatalytic activity of the Pt/C catalysts is enhanced by the thermal activation process. The EAS area increases from 11.2 to 56.8 m^2/g Pt with increasing activation time from 1 to 15 h. As compared to the E-TEK catalyst (54.9 m^2/g Pt), the Pt/C catalyst of 15 h shows only comparable EAS area (56.8 m^2/g Pt), and its utilization factor (93.4%) is much higher than that of the E-TEK (62.8%). The peak current densities increase with the activation time, demonstrating that the improvement of catalytic activity follows the extent of decomposition of $D400(EI)_{20}$ and the increase of the crystallinity of Pt demonstrated by XPS and XRD characterization.

Acknowledgment. We gratefully acknowledge the National Science Council, Taipei, Taiwan, for their generous financial support of this research.

Note Added after ASAP Publication. This article was published ASAP on May 2, 2006. A reference number was changed in the first paragraph of the Experimental Section. The revised version was reposted on May 3, 2006.

Supporting Information Available: Supplemental figures regarding the TGA thermogram and time-dependent weight loss curve (Figure S1). This material is available free of charge via the Internet at http://pubs.acs.org.

References and Notes

(1) Ding, Y.; Chen, M.; Erlebacher, J. *J. Am. Chem. Soc.* **2004**, *126*, 6876.
(2) Attard, G. S.; Leclerc, S. A. A.; Maniguet, S.; Russell, A. E.; Nandhakumar, I.; Bartlett, P. N. *Chem. Mater.* **2001**, *13*, 1444.
(3) Carrette, L.; Friedrich, K. A.; Stimming, U. *ChemPhysChem* **2000**, *1*, 162.
(4) Mukerjee, S.; Mcbreen, J. *J. Electroanal. Chem.* **1998**, *448*, 163.
(5) McNicol, B.; Rand, D.; Williams, K. *J. Power Sources* **1999**, *83*, 5.
(6) Watanabe, W.; Uchida, M.; Motoo, S. *J. Electroanal. Chem.* **1987**, *229*, 395.
(7) Schmidt, T. J.; Noeske, M.; Gasteiger, H. A.; Britz, P.; Bönnemann, H. *J. Electrochem. Soc.* **1998**, *145*, 925.
(8) Prabhuram, J.; Wang, X.; Hui, C. L.; Hsing, I. M. *J. Phys. Chem. B* **2003**, *107*, 11057.
(9) Kim, T.; Takahashi, M.; Nagai, M.; Kobayashi, K. *Electrochim. Acta* **2004**, *50*, 817.
(10) Wang, X.; Hsing, I. M. *Electrochim. Acta* **2002**, *47*, 2981.
(11) Liu, Z.; Ling, X. Y.; Lee, J. Y.; Su, X.; Gan, L. M. *J. Mater. Chem.* **2003**, *13*, 3049.
(12) Kuo, P. L.; Chen, W. F. *J. Phys. Chem. B* **2003**, *107*, 11267.
(13) Kuo, P. L.; Liang, W. J.; Wang, F. Y. *J. Polym. Sci., Part A: Polym. Chem.* **2003**, *41*, 1360.
(14) Manna, A.; Imae, T.; Aoi, K.; Okada, M.; Yogo, T. *Chem. Mater.* **2001**, *13*, 1674.
(15) Kuo, P. L.; Ghosh, S. K.; Liang, W. J.; Hsieh, Y. T. *J. Polym. Sci., Part A: Polym. Chem.* **2001**, *39*, 3018.
(16) Boehm, H. P.; Diehl, E.; Neck, W.; Sappok, R. *Angew. Chem., Int. Ed. Engl.* **1964**, *3*, 669.
(17) Boehm, H. *Carbon* **1994**, *32*, 759.
(18) Zang, F.; Srinivasan, M. P. *Langmuir* **2004**, *20*, 2309.
(19) Moulder, J. F.; Stick, W. F.; Sobol, P. E.; Bomben, K. D. *Handbook of X-ray Photoelectron Spectroscopy*; Perkin-Elmer: Eden Prairie, MN, 1992.
(20) Aricò, A. S.; Poltarzewski, Z.; Kim, H.; Morana, A.; Giordano, N.; Antonucci, V. *J. Power Sources* **1995**, *55*, 159.
(21) Pcuckert, M. *Electrochim. Acta* **1984**, *29*, 1315.
(22) Haimov, A.; Cohen, H.; Neumann, R. *J. Am. Chem. Soc.* **2004**, *126*, 11762.
(23) Sharma, J.; Mahima, S.; Kakade, A. B.; Pasricha, R.; Mandale, A. B.; Vijayamohanan, K. *J. Phys. Chem. B* **2004**, *108*, 13280.
(24) Adenier, A.; Chehimi, M. M.; Gallardo, I.; Pinson, J.; Vila, N. *Langmuir* **2004**, *20*, 8243.
(25) Hecq, A.; Delrue, J. P.; Hecq, M.; Robert, T. *J. Mater. Sci.* **1981**, *16*, 407.
(26) Sawyer, L. C.; Grubb, D. T. *Polymer Microscopy*, 2nd ed.; Chapman & Hall: New York, 1996.
(27) Luo, J.; Maye, M. M.; Han, L.; Kariuki, N. N.; Jones, V. W.; Lin, Y.; Engelhard, M. H.; Zhong, C. J. *Langmuir* **2004**, *20*, 4254.
(28) Shukla, A. K.; Neergat, M.; Bera, P.; Jayaram, V.; Hedge, S. M. *J. Electroanal. Chem.* **2001**, *504*, 111.
(29) Li, W.; Liang, C.; Zhou, W.; Qiu, J.; Zhou, Z.; Sun, G.; Xin, Q. *J. Phys. Chem. B* **2003**, *107*, 6292.
(30) Park, K. W.; Choi, J. H.; Kwon, B. K.; Lee, S. A.; Sung, Y. E.; Ha, H. Y.; Hong, S. A.; Kim, H. Y.; Wieckowski, A. *J. Phys. Chem. B* **2002**, *106*, 1869.
(31) Herrero, E.; Franaszczuk, K.; Wieckowski, A. *J. Phys. Chem. B* **1994**, *98*, 5074.
(32) Poizo, A.; De Francesco, M.; Cemmi, A.; Cardellini, F.; Giorgi, L. *J. Power Sources* **2002**, *105*, 13.
(33) Prabhuram, J.; Zhao, T. S.; Wong, C. W.; Guo, J. W. *J. Power Sources* **2004**, *134*, 1.
(34) Guo, J. W.; Zhao, T. S.; Prabhuram, J.; Wong, C. W. *Electrochim. Acta* **2005**, *50*, 1973.
(35) Hu, C. C.; Liu, K. Y. *Electrochim. Acta* **1999**, *44*, 2727.
(36) Xu, W.; Lu, T.; Liu, C.; Xing, W. *J. Phys. Chem. B* **2005**, *109*, 14325.
(37) Liu, Z.; Ling, X. Y.; Su, X.; Lee, J. Y. *J. Phys. Chem. B* **2004**, *108*, 8234.